



PD-1-expressing macrophages and CD8 T cells are independent predictors of clinical benefit from PD-1 inhibition in advanced mesothelioma

Krisztian Homicsko ^{1,2}, Panagiota Zygoura,³ Maxim Norkin,^{1,2} Stephanie Tissot,^{1,4} Nicholas Shakarishvili,¹ Sanjay Popat,⁵ Alessandra Curioni-Fontecedro,^{6,7} Mary O'Brien,⁸ Anthony Pope,⁹ Riyaz Shah,¹⁰ Patricia Fisher,¹¹ James Spicer ¹², Amy Roy,¹³ David Gilligan,¹⁴ Sylvie Rusakiewicz,⁴ Ekaterina Fortis,^{1,4} Nesa Marti,¹⁵ Roswitha Kammler,¹⁵ Stephen P Finn,¹⁶ Georges Coukos,^{1,2} Urania Dafni,^{3,17} Solange Peters,^{1,18} Rolf A Stahel¹⁹

To cite: Homicsko K, Zygoura P, Norkin M, *et al.* PD-1-expressing macrophages and CD8 T cells are independent predictors of clinical benefit from PD-1 inhibition in advanced mesothelioma. *Journal for ImmunoTherapy of Cancer* 2023;**11**:e007585. doi:10.1136/jitc-2023-007585

► Additional supplemental material is published online only. To view, please visit the journal online (<http://dx.doi.org/10.1136/jitc-2023-007585>).

Accepted 03 September 2023



© Author(s) (or their employer(s)) 2023. Re-use permitted under CC BY-NC. No commercial re-use. See rights and permissions. Published by BMJ.

For numbered affiliations see end of article.

Correspondence to

Dr Krisztian Homicsko;
krisztian.homicsko@chuv.ch

ABSTRACT

Background Few tissue biomarkers exist to date that could enrich patient with cancer populations to benefit from immune checkpoint blockade by programmed cell death protein 1/ligand-1 (PD-/L-1) inhibitors. PD-L1 expression has value in this context in some tumor types but is an imperfect predictor of clinical benefit. In malignant pleural mesothelioma, PD-L1 expression is not predictive of the benefit from PD-1 blockade. We aimed to identify novel markers in malignant pleural mesothelioma to select patients better.

Methods We performed a multiplex-immune histochemistry analysis of tumor samples from the phase III PROMISE-meso study, which randomized 144 pretreated patients to receive either pembrolizumab or standard second-line chemotherapy. Our panel focused on CD8+T cell, CD68+macrophages, and the expression of PD-1 and PD-L1 on these and cancer cells. We analyzed single and double positive cells within cancer tissues (infiltrating immune cells) and in the stroma. In addition, we performed cell neighborhood analysis. The cell counts were compared with clinical outcomes, including responses, progression-free and overall survivals.

Results We confirmed the absence of predictive value for PD-L1 in this cohort of patients. Furthermore, total CD8 T cells, CD68+macrophages, or inflammatory subtypes (desert, excluded, inflamed) did not predict outcomes. In contrast, PD-1-expressing CD8+T cells (exhausted T cells) and PD-1-expressing CD68+macrophages were both independent predictors of progression-free survival benefit from pembrolizumab. Patients with tumors simultaneously harboring PD1+T cells and PD-1+macrophages benefited the most from immune therapy.

Conclusion We analyzed a large cohort of patients within a phase III study and found that not only PD-1+CD8 T cells but also PD-1+CD68+ macrophages are predictive. This data provides evidence for the first time for the existence of PD-1+macrophages in mesothelioma and their clinical relevance for immune checkpoint blockade.

WHAT IS ALREADY KNOWN ON THIS TOPIC

⇒ Predictive biomarkers for programmed cell death protein 1 (PD-1) inhibitor therapy in mesothelioma and other solid tumors are lacking.

WHAT THIS STUDY ADDS

⇒ We found that PD-1 expression on CD68-positive macrophages and CD8-positive T cells predict progression-free survival from PD-1 inhibition. Furthermore, the concomitant presence of these cells provides a better prediction than either marker alone.

HOW THIS STUDY MIGHT AFFECT RESEARCH, PRACTICE OR POLICY

⇒ Our study shows the power of combined biomarkers for patient selection. These markers could be used to better select patients for PD-1 inhibitor therapy than existing markers, potentially increasing the level of survival benefit, and reducing exposure to those without benefit.

Immunotherapy became the standard of care for treating advanced malignant pleural mesothelioma (MPM).¹ A programmed cell death protein 1 (PD-1) inhibitor (pembrolizumab) was the first Food and Drug Administration-approved immunotherapy for selected malignant mesothelioma tumors with high tumor mutational burden.² Since then, the combination of ipilimumab and nivolumab has also been approved³ as frontline systemic therapy. However, only a fraction of patients experiences long-lasting benefits, defining an unmet need for better biomarkers to guide patient selection.⁴ The European Thoracic Oncology Platform (ETOP) has performed a

randomized phase III study (PROMISE-meso) in patients with pretreated MPM, comparing PD-1 blockade using pembrolizumab versus single-agent chemotherapy after failure of the first-line standard-of-care platinum-based chemotherapy.⁵ Patients treated with immunotherapy had a significantly higher rate of objective responses than those treated with chemotherapy (16/73 vs 4/71 responses; $p=0.004$). However, the groups had no significant difference in progression-free survival (PFS) or overall survival (OS). Importantly, Programmed cell death ligand 1 (PD-L1) expression was not associated with response or clinical benefit.⁵

The classical pathogenesis of MPM is due to the chronic inflammation induced by exposure to asbestos. The tumor mutation burden is typically very low in patients with MPM,⁶ although new studies using mate-pair sequencing found more mutations due to chromosomal rearrangements.⁷ Despite the low mutation burden and subsequent possibly low neoantigen load, MPMs have abundant CD8 T cell infiltrates,⁸ however, with signs of exhaustion, including PD-1, T-cell immunoglobulin and mucin-domain containing-3 (TIM-3), and lymphocyte-activation gene 3 (LAG-3) expression. The immune tumor microenvironment of MPM is dominated by myeloid cells, namely macrophages, and monocytes.⁹ The macrophages typically show an M2 polarization¹⁰ while monocytes are predominantly CD16^{Hi} non-classical monocytes.¹⁰ The myeloid cells create an immune suppressive microenvironment limiting the efficacy of immunotherapies.¹¹

The expression of PD-L1 on macrophages is well-established and is a marker of chronic inflammation.¹² In addition to PD-L1, tumor-associated macrophages might also express PD-1, as previously shown in colorectal cancer.¹³ Furthermore, exposure of PD-1-positive macrophages to a PD-1 inhibitor led to the increased phagocytic activity of macrophages,¹³ a potential alternative mechanism of action for PD-1 inhibitors beyond the reinvigoration of exhausted, antigen-specific CD8+T cells.¹⁴

This study aimed to identify baseline biomarkers that may characterize patient subgroups that could potentially benefit from immunotherapy. For this purpose, a multiparameter immunohistochemistry (IHC) analysis has been performed, focusing on the expression of PD-1 and PD-L1 on CD8+T cells, CD68+macrophages, and tumor cells.

RESULTS

The ETOP 9–15 PROMISE-meso study randomized 144 patients with immunotherapy naïve MPM after the failure of first-line chemotherapy to either pembrolizumab or chemotherapy, either gemcitabine or vinorelbine.⁵ Adequate tumor material was available from 64 of 73 (88%) patients in the pembrolizumab arm and 61 of 71 (86%) patients in the chemotherapy arm (figure 1A). The distribution of baseline characteristics for the 125 patients used in the current analysis is similar to the ones already presented for the full randomized cohort of

144 patients (online supplemental extended data table 1) No significant differences in baseline characteristics were evident between the treatment arms except for age ($p=0.020$) (online supplemental extended data table 1).

We performed a multiplex IHC analysis using the Vectra Polaris platform (see Methods). We stained slides for cancer cell markers (either calretinin or WT1) and CD3, CD8, CD68, PD-1, and PD-L1 (figure 1B). The distribution of biomarkers was not significantly different between the two treatment arms (online supplemental extended data table 2), using continuous variables or categories based on the adopted cut-offs presented in online supplemental extended data table 3. As expected, single and combined biomarkers were significantly correlated with each other (online supplemental extended data figure 1)

Tumor-infiltrating lymphocytes (TILs) are a subset of intratumor CD8+T cells that invade cancer tissue. We defined cancerous regions and surrounding stromal components for each sample and then measured CD8+T cells either within the cancer tissue (tumor CD8+) or within the stroma (stroma CD8+) (figure 1C). Using this approach, we could define tumors corresponding to the three general T cell inflammatory types of cancers: inflamed, excluded, or desert. Examples of inflammation subtypes are shown in Extended Data figure 2. We defined 10 CD8+T cells/mm² as a cut-off, corresponding to roughly two CD8+T cells per high power field. More than half of the tumors (68/125, 54%) showed a T cell inflamed phenotype. This is in accordance with previous reports showing high levels of CD8+TILs in MPM.⁸ Excluded phenotypes was shown in 21% of patients and desert phenotypes in 25% of patients. The TIL phenotypes were comparable between the two arms of the study, with no statistically significant difference ($p=0.78$) (figure 1D and online supplemental extended data table 2). We performed a similar analysis for macrophages as for CD8+T cells, defining CD68+cells within cancer cells and in the stroma. Approximately 10 times more macrophages were detected than CD8+T cells within cancer (tumor-infiltrating macrophages, TIMs) and the stroma (figure 1E).

We examined the association of individual biomarkers with outcomes. None of these could predict PFS or OS after false discovery rate (FDR) adjustment (online supplemental extended data table 4). Specifically, neither TIL inflammation types nor PD-1 and CD68+TIMs expression were associated with PFS estimates in patients treated with pembrolizumab (figure 1F, G and H, respectively). Similarly, no significant association of any biomarker with objective response rate (ORR) was identified after FDR adjustment (19 responses overall) (online supplemental extended data table 5).

We next looked at the subpopulation of cells according to PD-1 or PD-L1 expression status. Specifically, we looked at cancer infiltrating PD-1 or PD-L1 expressing CD3+, CD8+, and CD68+cells. Examples of PD-1-positive CD8+cells (CD8+PD-1+) and PD-1-positive CD68+ (CD68+PD-1+) cells are shown in figure 2A,B, respectively.

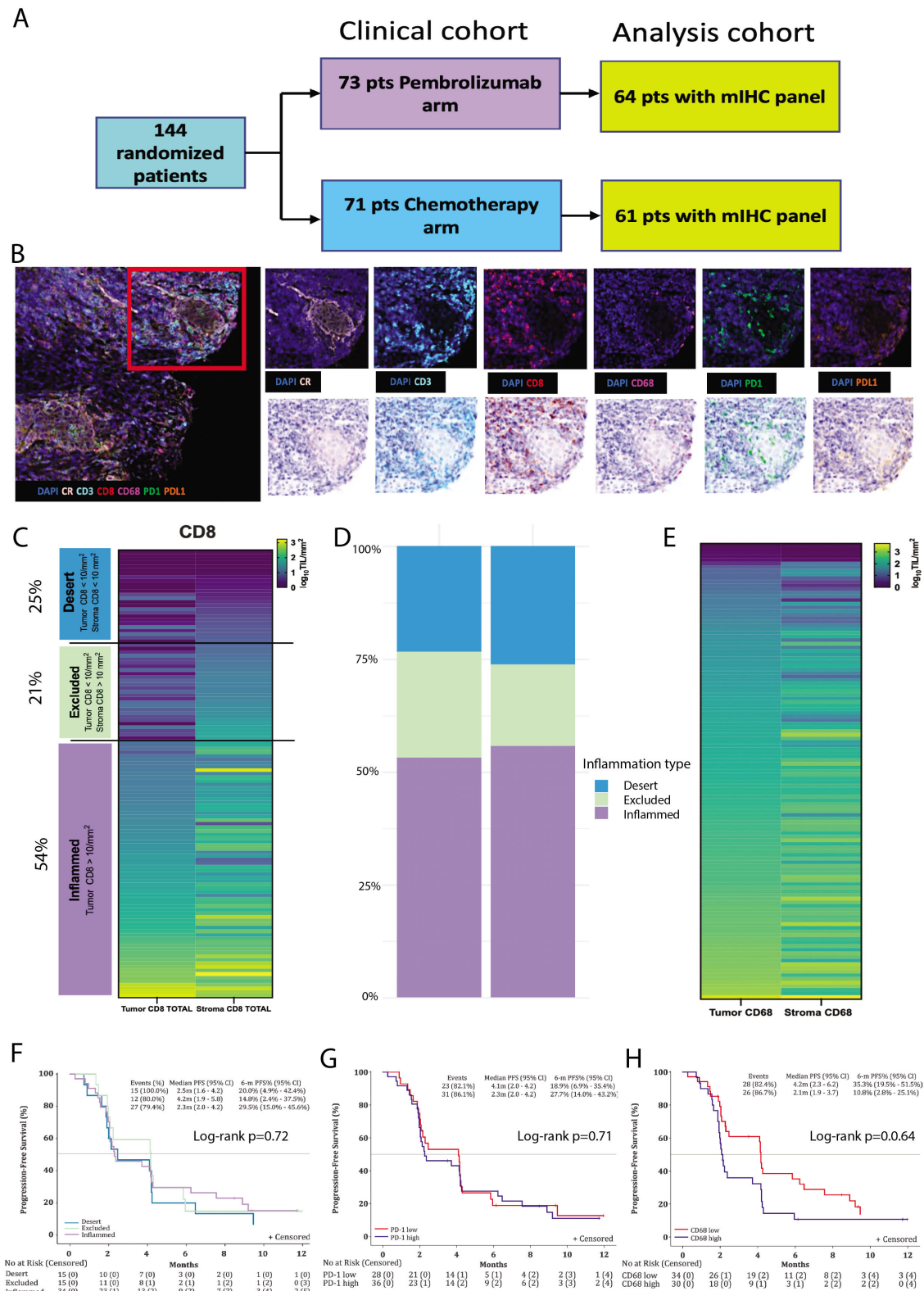


Figure 1 (A) Overview of the study and sample availability. (B) Representative images of multiplex IHC containing single staining for tumor cells (CR=calretinin or WT1), CD3, CD8, CD68, PD-L1, PD-1. (C) Heatmap of CD8 counts/mm² in tumor and stromal tissue represented on a log scale (Log₁₀ TIL/mm²). (D) Barplot of tumor inflammation types in the two arms of the study as defined in figure 1C. (E) Heatmap of CD68 counts/mm² in tumor and stromal tissue represented on a log scale (Log₁₀ TIL/mm²). (F) Kaplan-Meier estimates of PFS in the pembrolizumab arm of the study according to inflammation types as defined in figure 1C. (G) Kaplan-Meier estimates of PFS in the pembrolizumab arm of the study according to PD-1 levels. (H) Kaplan-Meier estimates of PFS in the pembrolizumab arm of the study according to CD68 cut-offs. mIHC, multiplex immunohistochemistry; PD-1, programmed cell death protein 1; PD-L1, programmed cell death protein 1/ligand-1; PFS, progression-free survival; pts, patients.

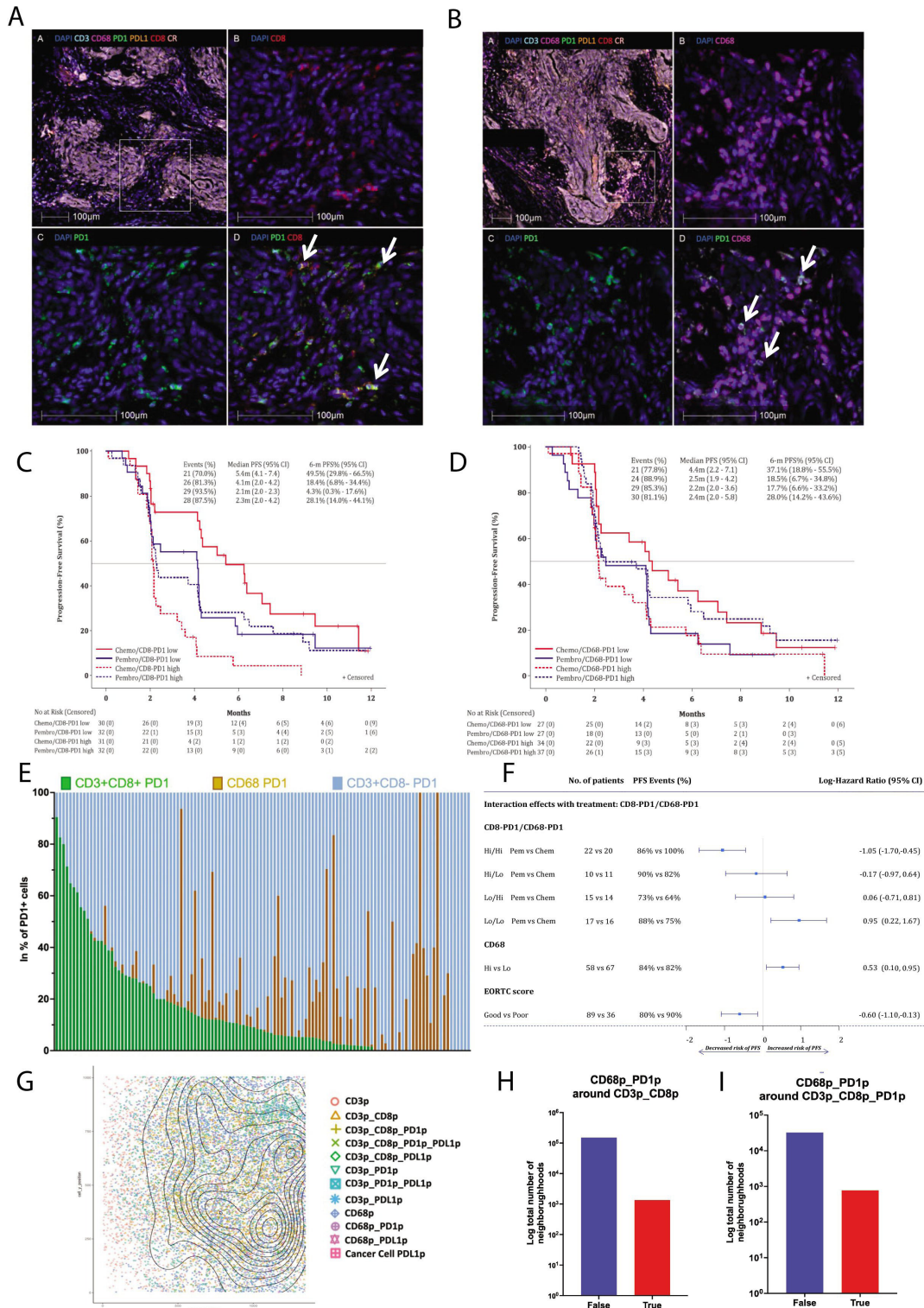


Figure 2 (A) Example of CD8+PD-1+ T cells in the tumor tissue. (B) Example of CD68+PD-1+ macrophages in the tumor tissue. (C) Kaplan-Meier estimates of PFS in both arms of the study according to CD8+PD-1+ cells low and high (cut-off value of $\geq 1/\text{mm}^2$). (D) Kaplan-Meier estimates of PFS in both arms of the study according to CD68+PD-1+ cells low and high (cut-off value of $>0/\text{mm}^2$). (E) Bar plot showing the distribution of cell types in PD-1+ cells for each patient. Each bar is a single patient. The percentage shows the relative frequency of CD3+CD8+, CD3+CD8-, and CD68+ cells. (F) Forest plot of log HRs of the final model for PFS after backward multivariable selection at 10%. Note: Interactions effects refer to interactions with treatment. Hi, high; Lo, low; Pem, pembrolizumab; Chem, chemotherapy. (G) Density map of kernel density estimation of selected cell types from the staining. The legend shows the cell types based on the combination of markers. (H) Barplot showing the absolute number of CD68+PD-1+ cells around CD3+CD8+ cells. (I) Barplot showing the absolute number of CD68+PD-1+ cells around CD3+CD8+PD-1+ cells. PD-1, programmed cell death protein 1; PD-L1, programmed cell death protein 1/ligand-1; PFS, progression-free survival.

We found approximately 12 times fewer CD8+PD-1+ T cells than total CD8+T cells, with a median of 1 CD8+PD-1+ cell/mm². Patients with high baseline PD-1-expressing CD8+T cells (≥ 1) randomized to pembrolizumab had significantly better PFS compared with those receiving chemotherapy ($HR_{\text{pembro_vs_chemo}} = 0.48$, 95% CI: 0.27 to 0.84), while the biomarker effect was reversed but non-significant in the cohort with low baseline PD-1-expressing CD8+T cells ($HR_{\text{pembro_vs_chemo}} = 1.60$, 95% CI: 0.88 to 2.89, interaction $p = 0.0043$; adjusted for clinical variables) (figure 2C and online supplemental extended data table 4). PD-1 expression is typically expected on T cells, notably on exhausted CD8+T cells, regulatory T cells (Tregs), and on effector memory and T helper 1 (Th1) cells. Our panel did not allow for the direct quantification of other T cell subtypes, notably CD4+ cells. However, we did detect PD-1 expression on T cells that did not stain for CD8 but only for CD3 (figure 2E). These cells could comprise both Th1 and Treg cells. Analysis of CD3+PD1+ but CD8- cells showed no correlation with PFS (online supplemental extended data table 8 and figure 4).

The existence of PD-1-positive macrophages remains controversial. We included Fc-blocking in all our experiments to exclude the possibility of non-specific binding of anti-PD-1 antibodies by Fc receptors of macrophages. The median abundance of CD68+PD-1+ cells was 160 times lower than the total number of macrophages, suggesting that the staining was specific and only present in a subset of macrophages. CD68+PD-1+ were also less frequent than CD8+PD-1+ T cells. We could still detect CD68+PD-1+ cells (at least one cell) in 56.8% of patients. Patients with high baseline PD-1-expressing CD68+ (> 0) randomized to pembrolizumab had a trend for improved PFS compared with those receiving chemotherapy ($HR_{\text{pembro_vs_chemo}} = 0.62$, 95% CI: 0.36 to 1.06). The effect of treatment on PFS differed between high and low CD68PD1 levels, with pembrolizumab associated with arithmetically longer PFS with high levels of CD68+PD1+, and worse PFS in low (interaction $p = 0.042$) (figure 2C and online supplemental extended data table 4).

To further investigate the association of PD-1+CD8+ and PD-1+CD68+ cells with PFS, a multivariable Cox model was developed, accounting for all biomarkers and co-expressions and adjusting for baseline clinical characteristics. Only the European Organisation for Research and Treatment of Cancer (EORTC) score was found significant ($p = 0.012$) among the latter. A significant interaction with treatment was found for CD8+PD-1+ ($p = 0.0093$) and CD68+PD-1+ cells ($p = 0.045$), while high CD68 expression (≥ 200) ($p = 0.014$) was found significant irrespective of treatment (figure 2F), thus suggesting a prognostic, but not predictive role. The interactions indicate that the impact on treatment differs depending on the baseline CD8+PD-1+ and CD68+PD-1+ (figure 2C,D). As shown in figure 2F, patients with both high CD8+PD-1+ and CD68+PD-1+ at baseline randomized to pembrolizumab had significantly better PFS compared with those receiving chemotherapy ($n = 42$, $HR_{\text{pembro_vs_chemo}} = 0.35$, 95% CI: 0.19 to 0.64). On the other hand,

chemotherapy had a beneficial effect in terms of PFS for patients with both low CD8+PD-1+ and CD68+PD-1+ ($n = 33$, $HR_{\text{pembro_vs_chemo}} = 2.58$, 95% CI: 1.25 to 5.31). The association of CD8+PD-1+ cells with PFS was significant in the individual marker analysis (online supplemental extended data table 4), consistent with a sensitivity analysis using the continuous measurements for the biomarkers (online supplemental extended data table 6).

Although we did not find significant effects on OS assessing markers individually, when we explored all markers together in a multivariable analysis, associations with OS were detected. Interactions of treatment with CD68+PD-1+ ($p = 0.015$) and cancer cell PD-L1 expression ($p = 0.033$) were identified along with general CD68 expression ($p = 0.016$). For the CD68+PD-1+ biomarker, the differential treatment effect on OS was in the same direction as found for PFS, that is, for better outcomes. Other baseline clinical variables that were found to be associated with OS were sex ($p = 0.043$), EORTC score ($p < 0.001$), and prior treatment ($p = 0.014$) (online supplemental extended data table 7).

The PROMISE-MESO study also collect whole blood RNA samples, pretreatment and on-treatment (Cycle 2, Day 1). In order to define potential correlation between intratumoral and systemic immunity, we analyzed the whole blood RNA samples using RNA sequencing followed by deconvolution with CibersortX and pathway analysis. Specifically, we measure the relative abundance of Tregs, CD4-positive cell types, and CD8 T cells. We found no correlation between patients with CD8+PD1+ (online supplemental extended data figure 3A) and CD68+PD1+ tumors and blood deconvolution (online supplemental extended data figure 3B). We also measured signaling pathways of interferon gamma (INF γ), interleukin-6 (IL-6), and interleukin-8 (IL-8) (online supplemental extended data figure 3C). In baseline samples, INF γ signature in whole blood RNA sequencing was higher in patients with CD68+PD1 positive tumors but not CD8PD1+ tumors. IL-6 and IL-8 signatures at baseline were not higher in CD68+PD1+ or CD8+PD1+ tumors. Interestingly, we found that in on-treatment blood samples, the IL-8 signature was higher in CD8+PD+ patients, and a similar trend was detected for IL-6. However, no similar difference was detected in on-treatment samples for CD68+PD1+ patients.

Finally, we aimed to exclude that PD-1 staining might be an artifact from the proximity of CD8+ and CD68+ cells expressing PD-1. To this end, we used the segmented images and calculated the number of CD68+PD-1+ cells in the immediate neighborhood of CD8+ cells or CD8+PD-1+ cells (figure 2G). We found an absence of enrichment of CD68+PD-1+ cells in the proximity of CD8+ cells (CD3p_CD8p), or CD8+PD-1+ cells (CD3p_CD8p_PD1p) (figure 2H,I, respectively).

DISCUSSION

Predictive biomarkers for immunotherapy of patients with MPM are still elusive. The expectation is that biomarkers

shall identify a subset of patients who benefit from immunotherapy but, importantly, spare patients who will not benefit to minimize morbidity from immune-mediated adverse events and significant financial toxicities.¹⁵ In addition, biomarkers should be simple and robust enough and reproducible to be applicable in clinical settings. In MPM, PD-L1 alone does not allow for patient selection.^{3 5 16 17} Our analyses do not suggest an association between PD-L1 expression on cancer cells and PFS, although it was found to be an independent predictive factor in the multivariable model for OS (online supplemental extended data table 7). However, this association was not identified in the analysis of individual biomarkers (online supplemental extended data table 4) or in the sensitivity analysis using continuous measurements (online supplemental extended data table 6).

The presence of T cells, especially CD8+T cells, which are expected to be mechanistically linked to activation by PD-1 or PD-L1 blockade, has been explored as a potential biomarker for immune checkpoint blockade. A meta-analysis had previously shown that the presence of CD8+cells could predict outcomes, although with a large variability of impact according to tumor types.¹⁸ The same study also found that the location of CD8+T cells (inflamed, excluded, or desert) did not provide value for patient selection, matching our results in MPM. CD8+T cells comprise multiple subtypes. After antigen exposure, effector T cells could become exhausted and express inhibitory markers like PD-1, LAG-3, and TIM-3.¹⁹ Mechanistically, CD8+PD-1+ cells are the direct targets of PD-1 inhibitors. However, our analysis showed that not only CD8+PD-1 cells but also CD68+PD-1 cells are critical. The combined presence of high CD8+PD-1 and high CD68+PD-1 is associated with the best PFS in patients receiving pembrolizumab instead of chemotherapy (n=42, $HR_{\text{pembro_vs_chemo}}=0.35$, 95% CI: 0.19 to 0.64). In contrast, for the cohort of patients with low biomarkers, the PFS risk is significantly increased when receiving pembrolizumab versus chemotherapy (n=33, $HR_{\text{pembro_vs_chemo}}=2.58$, 95% CI: 1.25 to 5.31). This is consistent with the observed continuous trend from low to high risk when only one of these biomarkers is present at baseline (figure 2F). Our data confirm that the presence of CD8+PD-1+ T cells is associated with PFS from PD-1 inhibitors over single-agent chemotherapy. Interestingly, we also found that the presence of these cells is a strong negative predictor of PFS from chemotherapy, whereas patients with low CD8+PD-1+ cells seem to benefit more from chemotherapy. This result also suggests that biomarkers for PD-1 immunotherapy might have the opposite impact on chemotherapy and, thus, the combination of immune therapy and chemotherapy may not necessarily need to be given to all patients.

The clinical impact of PD-1-expressing macrophages has not been elucidated to date. Our publication is the first to confirm the potential association of PD-1+macrophages on PD-1 inhibitor therapy. This data suggests that PD-1 therapy might activate T cells and macrophages to

drive clinical benefit. The increased impact of the combination of PD-1 expressing CD8+ and CD68+ cells further underscores the added value of these macrophages as potential biomarkers.

Together, PD-1-expressing CD8+Tcells and PD-1-expressing CD68+macrophages could be predictors of benefit from immunotherapies and of lack of benefit from chemotherapy. As our study is retrospective and exploratory, we expect that additional analyses in larger cohorts of patients could validate these markers.

MATERIAL AND METHODS

Study design and translational objectives

This exploratory translational analysis was based on patients randomized in the ETOP 9–15 PROMISE-meso trial. ETOP 9–15 PROMISE-meso is an open-label, randomized international phase III trial. The primary objective of the study was to demonstrate a benefit in terms of PFS with the use of pembrolizumab compared with standard, institutional-choice chemotherapy (gemcitabine or vinorelbine) in patients with advanced malignant mesothelioma who failed first-line chemotherapy and were naïve to immunotherapy. The trial design, details, and outcomes have been previously published.⁵

The aim of the current study was to explore the prognostic and predictive role of biomarkers on the tumors collected before the start of treatment. Specifically, the aim was to identify subgroups of patients that could potentially derive benefit from immunotherapy with pembrolizumab. The participating patients signed the study consent form that permitted translational research analyses.

Tissue material

The translational analysis includes tumor tissue available from 125 patients randomized in the ETOP 9–15 PROMISE-meso phase III trial (total randomized: 144). The stratification factor used in this clinical trial was the histological subtype (predominately epithelioid vs non-epithelioid). The availability of tumor tissue, whole blood, and serum samples for translational research was part of the inclusion criteria for this trial. Biological material was collected at baseline from all randomized patients and was submitted to, cataloged, and maintained at a central laboratory. Tumor tissue blocks, whole blood, and serum samples were centrally collected and biobanked at the ETOP Biobank, located at the Center for Experimental Therapeutics CTE, CHUV Lausanne, Switzerland. The collected material was subject to a central histology review.

Multispectral immunofluorescence staining

Multiplexed staining was performed on 4-micrometer formalin-fixed paraffin-embedded tissue sections on the automated Ventana Discovery Ultra staining module (Ventana, Roche). Slides were placed on the staining module for deparaffinization, epitope retrieval (64 min at

95°C), and endogenous peroxidase quenching (Discovery Inhibitor, 8 min, Ventana).

Multiplex staining consists of multiple rounds of staining. Each round includes non-specific site blocking (Discovery Goat IgG and Discovery Inhibitor, Ventana), primary antibody incubation, secondary horseradish peroxidase (HRP)-labeled antibody incubation for 16 min (Discovery OmniMap anti-rabbit HRP (Ventana, # 760–4311) or anti-mouse HRP (Ventana, #760–4310)), OPAL reactive fluorophore detection (Akoya Biosciences, Marlborough, Massachusetts, USA) that covalently label the primary epitope (incubation: 12 min) and then antibodies heat denaturation. Sequence of antibodies used in the multiplex with the associated OPAL are the following: first: mouse monoclonal anti-human PD-1 antibody (clone NAT105, dilution 1:100 Biocare, 1 hour, room temperature (RT)), OPAL570 ; second: rabbit monoclonal anti-PD-L1 antibody (4 µg/mL, clone E1L3N, dilution 1:100, Cell Signaling, 1 hour, RT), OPAL620; third: rabbit polyclonal anti-human CD3 antibody (dilution 1:400, Dako, 1 hour, 37°C), OPAL520 ; fourth: mouse monoclonal anti-CD68 antibody (dilution 1:500, clone PG-M1, 1 hour, 37°C), OPAL540 ; fifth: rabbit monoclonal anti-calretinin (clone SP65, Ready-to-used Roche antibody, 1 hour, RT) or mouse polyclonal WT1 (Ready-to-used Roche antibody, 1 hour, RT), OPAL690 ; sixth: rabbit anti-CD8 antibody (dilution 1:800, clone SP16, Cellmarque, 1 hour, 37°C), OPAL 650. Nuclei were visualized by a final incubation with Spectral DAPI (1/10, FP1490, Akoya Biosciences) for 12 min. Multiplex immune fluorescence (mIF) images were acquired on Vectra V.3.0 automated quantitative pathology imaging system (Akoya Biosciences). Tissue and panel-specific spectral library of each panel individual fluorophore and tumor tissue autofluorescence were acquired for an optimal IF signal unmixing (individual spectral peaks) and multiplex analysis. IF stained slides were pre-scanned at 10× magnification. Using the Phenochart whole-slide viewer (Akoya Biosciences). The whole tumor is selected and annotated for the high-resolution multispectral acquisition of images at 20× magnification. IF signal extractions were performed using, inForm V.2.3.0 image analysis software (Akoya Biosciences), enabling a per-cell analysis of IF markers of multiplex stained tissue sections. The images were first segmented into tumor, stroma, and necrosis regions, based on the calretinin or WT1 staining using the inForm Tissue Finder algorithms. Individual cells were then segmented using the counterstained-based cell segmentation algorithm based on DAPI staining. Quantification of the immune cells is performed using the inForm active learning phenotyping algorithm by assigning the different cell phenotypes across several images. IF-stained cohorts are then batch processed, and data were exported and processed via an in-house developed R-script algorithm to retrieve every cell population.

T cell inflammation subtypes were defined based on CD8 T cell counts in the stroma and cancer tissue. We defined the cut-off of ten CD8+cells/mm² as a cut-off for

cancer tissue (tumor infiltrating CD8 cells) and stroma (stroma infiltrating T cells). We then combined these values to define inflamed (≥10 CD8 positive cells/mm² in cancer tissue, irrespective of stroma), excluded (CD8<10 cells/mm² in cancer tissue but ≥10 cells/mm² in the stroma), and desert (<10 CD8 cells mm² both in cancer and stromal tissues). Three representative cases of each of the three inflammatory types are provided in Extended data figure 2.

Cell density calculation

For each slide from each patient, we have multiple regions of interests (ROIs), and for each ROI, we collected information on the surface of the tumor and stroma (mm²). Moreover, we have information regarding each cell and its location in the stroma or tumor. We compute the densities by counting the number of cells, of a specific phenotype, in each tissue type for each ROI. The final density of a specific phenotype for a specific tissue for a specific patient is computed by averaging the values of density for each ROI.

Distance analysis

The cohort contains the coordinates for each cell on an x/y distribution. By using this information, one can generate metrics that give the proximity between any type of phenotypes that are of interest in the study.

In this study, we used a “Single Neighbor Metric” (now on SNM) to characterize the interaction between two species.

We can imagine two species, A and B as two sets with elements $A = (1, \dots, n)$ and $B = (1, \dots, n)$.

An element of set A will have coordinates a, and an element of set B will have coordinates b, b.

The distance between two elements of each set is defined as the Euclidean distance:

$$d = \sqrt{(x_a - x_b)^2 + (y_a - y_b)^2}$$

By using the Euclidean distance, we could measure, for instance, the number of elements of B around a given element A in a given radius μ .

We define a function S that is applied to an element of the set A (or B) and gives the number of elements of the set B (or A) that are closer than the distance μ .

$$S(A_i) = \sum_{k=1}^n \begin{cases} 1, & \text{if } d(A_i, B_k) < \mu \\ 0, & \text{otherwise} \end{cases}$$

Applying this function to each element of A gives us an array with values between 0 and n, where the value of such array tells us how many neighbors such element has.

We can call such array S_{A_i} and we can apply a second function N:

$$N(S_{A_i}) = \begin{cases} 1, & \text{if } S_{A_i} > 0 \\ 0, & \text{otherwise} \end{cases}$$



We obtain a final array that we will call N_{BA_i} with values either 0 or 1 for each element of A. Such an array can already be used to produce images to show how many cells of a given phenotype have at least one neighbor of a target phenotype. We can compute the metric SNM of B around A just by computing the average of the arrays N_{BA_i} . This value can be interpreted as the average proximity of B to A. Such a value ranges between 0 and 1. Zero means no proximity or that there is not a single element of set B at a distance less than μ from any element of set A. One means maximum proximity or that there is at least one element of set B at a distance less than μ for each element of set A.

We can apply this procedure to each pair of phenotypes of interest, and we can consider the origin of the tissue of one of the pairs. For instance, we can measure the SNM for CD3+CD8+ (from any tissue type) to CD68+PD-1+ in tumor.

We could imagine that there will be events where we have a cell of phenotype CD68+PD-1+ that resides in the tumor tissue but has, as a neighbor, a cell of type CD3+CD8+ that resides in the stroma.

Statistical analysis

Baseline tumor measurements of a panel consisting of five biomarkers (CD3, CD8, CD68, PD-1, PD-L1) and the co-expression of the first three with either PD-1 or PD-L1 (six co-expressions) were analyzed to explore their association with patient outcome. The association of inflammation type with outcome was also explored (inflamed, excluded, and desert type, based on a CD8 cut-off of 10 in tumor and stroma) (online supplemental extended data table 2). To account for multiple testing, the FDR method²⁰ was implemented to adjust for the 12 alternative tests (11 biomarkers and co-expressions and inflammation type).

Between-marker associations were explored by the Spearman correlation coefficient (S). Biomarker and co-expression values were categorized with thresholds chosen based on literature or unsupervised cut-offs (online supplemental extended data table 3). Clinical baseline patient characteristics (sex, age at randomization, histological subtype, smoking history, Eastern Cooperative Oncology Group performance status (ECOG PS), EORTC prognostic score, and prior treatment) were included in multivariable analyses to explore their association with PFS and OS.

The balance of baseline characteristics and biomarkers between the two treatment groups was tested by Fisher's exact and Mann-Whitney tests for categorical and continuous variables, correspondingly. PFS and OS rates were estimated by the Kaplan-Meier method. Potential differences in ORR by biomarker levels were assessed within each arm, according to Fisher's exact test, and overall for all randomized patients, based on the Breslow test for homogeneity between arms and Cochran-Mantel-Haenszel (CMH) test stratified by the arm (the CMH test was applicable only in cases where the Breslow test did

not reject the hypothesis of homogeneity between the treatment arms).

Cox proportional hazards regression for PFS and OS, separately for each biomarker, in the presence of treatment and treatment interaction, adjusted for baseline clinical variables, was the main analysis tool to assess the prognostic or predictive effect of categorized biomarkers and co-expressions (based on the adopted cut-offs). Multivariable models were stratified by histological subtype and also adjusted for sex, age at randomization, smoking history, ECOG PS, EORTC score, and prior treatment. The backward elimination method, with a removal criterion at 10%, was implemented to select variables remaining in the model, including interactions of inflammation type and each biomarker by treatment. Adjustment for the treatment arm was present in the final multivariable models run in the full study population. In the multivariable analysis, only predictors included in the final model and significant at 5% are described. A sensitivity analysis was performed for the model selection for PFS and OS, where Cox models, stratified by histology, were run for each biomarker (or co-expression) of interest using the continuous measurements, as well as its interaction with treatment. Models were also adjusted for other baseline characteristics after the backward elimination method with a 10% removal criterion. HRs and corresponding 95% CIs were obtained from the final chosen Cox model for the categorical biomarkers. Deviations from the proportionality assumption were assessed using the Schoenfeld residuals. All p values reported for PFS and OS correspond to the Wald test from stratified Cox models. All p values are considered significant at the 0.05 level. The statistical analysis was implemented using SAS V.9.4.

Study approval

The study was performed in Spain, Switzerland and the UK.

Author affiliations

¹Department of Oncology, Centre Hospitalier Universitaire Vaudois, Lausanne, Switzerland

²Ludwig Institute for Cancer Research, Lausanne branch, Lausanne, Switzerland

³ETOP Statistical Center, Frontier Science Foundation - Hellas, Athens, Greece

⁴Immune Landscape Laboratory, Centre Thérapies Expérimentales (CTE), Centre Hospitalier Universitaire Vaudois, Lausanne, Switzerland

⁵Lung Unit, Royal Marsden Hospital NHS Trust, London, UK

⁶Faculty of Science and Medicine, University of Fribourg, Fribourg, Switzerland

⁷Department of Oncology, Fribourg Hospitals, Fribourg, Switzerland

⁸Department of Oncology, Royal Marsden Hospital NHS Trust, London, UK

⁹Department of Oncology, Clatterbridge Cancer Centre NHS Foundation Trust, Bebington, UK

¹⁰Department of Medical Oncology, Kent Oncology Centre, Maidstone, UK

¹¹Department of Medical Oncology, Weston Park Hospital, Sheffield, UK

¹²Comprehensive Cancer Center, King's College London, London, UK

¹³Department of Medical Oncology, University Hospitals Plymouth NHS Trust, Plymouth, UK

¹⁴Department of Medical Oncology, Addenbrooke's Hospital, Cambridge, UK

¹⁵Translational Research Coordination, ETOP IBCSG Partners Foundation, Bern, Switzerland

¹⁶Molecular Diagnostics and Histopathology, Trinity College, Dublin, Ireland

¹⁷National and Kapodistrian University of Athens, Athens, Greece

¹⁸Agora Research Center, Swiss Cancer Center Leman, Lausanne, Switzerland

¹⁹President, ETOP IBCSG Partners Foundation, Bern, Switzerland

Twitter Sanjay Popat @DrSanjayPopat

Acknowledgements The ETOP 9-15 PROMISE-meso trial was sponsored by the ETOP IBCSG Partners Foundation and coordinated in collaboration with the Spanish Lung Cancer Group (SLCG) and the Swiss Group for Clinical Cancer Research (SAKK) with the financial support of Merck Sharp & Dohme and the Swiss National Accident Insurance Fund (SUVA). This translational subproject was sponsored and coordinated by the ETOP IBCSG Partners Foundation.

Contributors KH: Study conception & design, acquisition, Analysis, Interpretation of data, writing, guarantor of the overall content of the study, PZ, SP, AC-F, TP, RS, PF, JS, AR, DG, NM, RK, SPF, UD, SP, RAS: Study conception & design, analysis, interpretation of data, writing. ST: Analysis, interpretation of data, writing, MN: Acquisition, analysis, Interpretation of data, writing. NS, MO: Acquisition, interpretation of data, writing. CV: Acquisition, interpretation of data, writing. GC: Study conception & design, Interpretation of data, writing

Funding The funding was provided by the European Thoracic Oncology Platform from the ETOP IBCSG Partners Foundation.

Competing interests KH: Grant support: MSD, Roche, BMS, Molecular Partners, Travel grant: BMS, MSD, Astra-Zeneca. MO: Ad boards for MSD and Roche. RS: Ad board for MSD, Merck and Pierre Fabre.

Patient consent for publication Not applicable.

Ethics approval All patients, whose biological material and clinical data was included in our translational research study, signed an informed consent for the PROMISE-meso clinical trial and thereby consented that the biological material and clinical data collected as part of the PROMISE-meso clinical trial, may be used for translational mesothelioma research. The ETOP 9-15 PROMISE-meso trial was conducted in adherence to all country-specific ethics and regulatory requirements. The study was run in three European countries: Spain, Ethics approval ID AC022/17; Switzerland, BASEC-Nr 2016-02144; UK REC reference: 17/SC/0231. Participants gave informed consent to participate in the study before taking part.

Provenance and peer review Not commissioned; externally peer reviewed.

Data availability statement Data are available upon reasonable request. Images can be provided upon reasonable request. RNA sequencing data will be made available.

Supplemental material This content has been supplied by the author(s). It has not been vetted by BMJ Publishing Group Limited (BMJ) and may not have been peer-reviewed. Any opinions or recommendations discussed are solely those of the author(s) and are not endorsed by BMJ. BMJ disclaims all liability and responsibility arising from any reliance placed on the content. Where the content includes any translated material, BMJ does not warrant the accuracy and reliability of the translations (including but not limited to local regulations, clinical guidelines, terminology, drug names and drug dosages), and is not responsible for any error and/or omissions arising from translation and adaptation or otherwise.

Open access This is an open access article distributed in accordance with the Creative Commons Attribution Non Commercial (CC BY-NC 4.0) license, which permits others to distribute, remix, adapt, build upon this work non-commercially, and license their derivative works on different terms, provided the original work is properly cited, appropriate credit is given, any changes made indicated, and the use is non-commercial. See <http://creativecommons.org/licenses/by-nc/4.0/>.

ORCID iDs

Krisztian Homicsko <http://orcid.org/0000-0003-0912-6198>

James Spicer <http://orcid.org/0000-0003-3732-8491>

REFERENCES

- Fennell DA, Dulloo S, Harber J. Immunotherapy approaches for malignant pleural Mesothelioma. *Nat Rev Clin Oncol* 2022;19:573–84.
- Marabelle A, Le DT, Ascierto PA, *et al.* Efficacy of Pembrolizumab in patients with Noncolorectal high Microsatellite instability/mismatch repair-deficient cancer: results from the phase II KEYNOTE-158 study. *J Clin Oncol* 2020;38:1–10.
- Baas P, Scherpereel A, Nowak AK, *et al.* First-line Nivolumab plus Ipilimumab in Unresectable malignant pleural Mesothelioma (Checkmate 743): a Multicentre, randomised, open-label, phase 3 trial. *Lancet* 2021;397:375–86.
- Yang H, Xu D, Schmid RA, *et al.* Biomarker-guided targeted and Immunotherapies in malignant pleural Mesothelioma. *Ther Adv Med Oncol* 2020;12:1758835920971421.
- Popat S, Curioni-Fontecedro A, Dafni U, *et al.* A Multicentre randomised phase III trial comparing Pembrolizumab versus single-agent chemotherapy for advanced pre-treated malignant pleural Mesothelioma: the European Thoracic oncology platform (ETOP 9-15) PROMISE-Meso trial. *Ann Oncol* 2020;31:1734–45.
- Hmeljak J, Sanchez-Vega F, Hoadley KA, *et al.* Integrative molecular characterization of malignant pleural Mesothelioma. *Cancer Discov* 2018;8:1548–65.
- Mansfield AS, Peikert T, Smadbeck JB, *et al.* Neoantigenic potential of complex Chromosomal Rearrangements in Mesothelioma. *J Thorac Oncol* 2019;14:276–87.
- Marcq E, Siozopoulou V, De Waele J, *et al.* Prognostic and predictive aspects of the tumor immune Microenvironment and immune checkpoints in malignant pleural Mesothelioma. *Oncoimmunology* 2017;6:e1261241.
- Chu GJ, van Zandwijk N, Rasko JEJ. The immune Microenvironment in Mesothelioma: mechanisms of resistance to Immunotherapy. *Front Oncol* 2019;9:1366.
- Chéné A-L, d'Almeida S, Blondy T, *et al.* Pleural effusions from patients with Mesothelioma induce recruitment of monocytes and their differentiation into M2 Macrophages. *J Thorac Oncol* 2016;11:1765–73.
- Mantovani A, Allavena P, Marchesi F, *et al.* Macrophages as tools and targets in cancer therapy. *Nat Rev Drug Discov* 2022;21:799–820.
- Shinchi Y, Ishizuka S, Komohara Y, *et al.* The expression of PD-1 ligand 1 on Macrophages and its clinical impacts and mechanisms in lung adenocarcinoma. *Cancer Immunol Immunother* 2022;71:2645–61.
- Gordon SR, Maute RL, Dulken BW, *et al.* PD-1 expression by tumor-associated Macrophages inhibits Phagocytosis and tumor immunity. *Nature* 2017;545:495–9.
- Lee J, Ahn E, Kissick HT, *et al.* Reinvigorating exhausted T cells by blockade of the PD-1 pathway. *Forum Immun Dis Ther* 2015;6:7–17. 10.1615/ForumImmunDisTher.2015014188 Available: <http://www.dl.begellhouse.com/journals/1a654bf03faf67ac,5e042bea1b68dc83.html>
- Spencer KR, Wang J, Silk AW, *et al.* Biomarkers for Immunotherapy: Current developments and challenges. *Am Soc Clin Oncol Educ Book* 2016;35:e493–503.
- Disselhorst MJ, Quispel-Janssen J, Lalezari F, *et al.* Ipilimumab and Nivolumab in the treatment of recurrent malignant pleural Mesothelioma (INITIATE): results of a prospective, single-arm, phase 2 trial. *Lancet Respir Med* 2019;7:260–70.
- Fennell DA. Programmed death 1 blockade with Nivolumab in patients with recurrent malignant pleural Mesothelioma. *J Thorac Oncol* 2018;13:1436–7.
- Li F, Li C, Cai X, *et al.* The association between Cd8+ tumor-infiltrating lymphocytes and the clinical outcome of cancer Immunotherapy: A systematic review and meta-analysis. *EClinicalMedicine* 2021;41:101134.
- Haymaker C, Wu R, Bernatchez C, *et al.* “PD-1 and BTLA and Cd8+ T-cell “exhaustion” in cancer”. *Oncoimmunology* 2012;1:735–8.
- Baggio L, Prodi GA. False discovery rate: setting the probability of false claim of detection. *Class Quantum Grav* 2005;22:S1373–9.